PNAS RESEARCH ARTICLE | ENGINEERING

Antimicrobial second skin using copper nanomesh

Jae Joon Kim[a,1], Siyoung Ha[b,1], Lina Kim[b], Yutaro Kato[a], Yan Wang[a], Chihiro Okutani[a], Haoyang Wang[a], Chunya Wang[a], Kenjiro Fukuda[c], Sunghoon Lee[a], Tomoyuki Yokota[a], Oh Seok Kwon[b,d,2], and Takao Someya[a,c,2]

Edited by John Rogers, Northwestern University, Evanston, IL; received January 16, 2022; accepted April 13, 2022

The functional support and advancement of our body while preserving inherent naturalness is one of the ultimate goals of bioengineering. Skin protection against infectious pathogens is an application that requires common and long-term wear without discomfort or distortion of the skin functions. However, no antimicrobial method has been introduced to prevent cross-infection while preserving intrinsic skin conditions. Here, we propose an antimicrobial skin protection platform copper nanomesh, which prevents cross-infectionmorphology, temperature change rate, and skin humidity. Copper nanomesh exhibited an inactivation rate of 99.99% for *Escherichia coli* bacteria and influenza virus A within 1 and 10 min, respectively. The thin and porous nanomesh allows for conformal coating on the fingertips, without significant interference with the rate of skin temperature change and humidity. Efficient cross-infection prevention and thermal transfer of copper nanomesh were demonstrated using direct on-hand experiments.

antimicrobial performance | copper coating | nanofiber mesh | breathability | cross-infection prevention

Significance

The recent COVID-19 pandemic requires long-term and real-life applicable antimicrobial skin protection. However, there has been no practical solution to prevent cross-infection while preserving intrinsic skin naturalness. Conventional blocking-based approaches such as gloves cannot preserve the skin sterility and modify the morphology, temperature change rate, and humidity affecting our sensation and comfort. Here, we propose a skin-attachable protection platform copper nanomesh, which prevents cross-infection while maintaining skin naturalness. Copper nanomesh composed of copper coating and interconnected polymer nanofibers kills 99.99% of bacteria and viruses within 1 and 10 min and prevents bacterial cross-infection. The thin and porous structure of the nanomesh enables natural skin-environment interaction in terms of the morphology, temperature change rate, and humidity compared to films or gloves.

The functional support and advancement of our body while preserving the inherent naturalness is one of the ultimate goals of bioengineering (1–4). A functional layer is placed on the skin to complement the intrinsic biological and interactive functions (5, 6) and to add functions that do not yet exist (7–9). During use, the second skin layer should completely exploit its function and underlay skin functions without deforming the skin or interfering with the skin's external interaction. Materials and structures need to be conformal and mechanically similar to the skin to minimize the distortion of natural sensations and movements. In addition, the air and heat transfer on the skin must be unimpeded to obtain a natural and comfortable wear fit (10).

Body protection that requires common and long-term wear is an application in which both functionality and naturalness are important. As the outermost layer connecting our body to the environment, the skin is exposed to physical damage, hazardous chemicals, and infectious pathogens (11, 12). Therefore, we add a protective layer on the skin that blocks or filters out external contaminants. This entails the isolation and accumulation of biochemical compounds, which can lead to self-contamination and the subsequent cross-contamination/infection by interacting with other objects. In contrast to chemical contamination, which is not self-reproductive, the biological contamination of infectious microbes, such as severe acute respiratory syndrome coronavirus 2 (SARS-CoV-2), is a considerable issue to be addressed.

By containing an antimicrobial material on the surface of the skin protective layer, cross-infection can be prevented in the long term. Unlike temporary rinsing or disinfection, the use of antibacterial or antiviral substances such as chemical or natural disinfectants and metal nanomaterials inhibits the growth of microorganisms on the surface (13–17). These materials are embedded in a complete covering polymer layer, such as gloves (18, 19), to isolate and protect both the inner and outer surfaces from the infection. To add breathability to the textile especially for the mask (13, 20, 21), many antibacterial fibers have been developed based on these materials. Moreover, various skin-attachable platforms with antimicrobial properties have been developed for convenient usage in daily lives. Antimicrobial nanofibers with conformal attachment to the skin have been developed for drug delivery, wound healing (22, 23), and electrophysiology (24, 25). In addition, stretchable and antibacterial hydrogels have been developed to allow more natural skin movement in wound-healing applications (26–28).

However, there has been no practical skin protective solution to prevent cross-infection while preserving intrinsic skin conditions such as surface morphology, thermal transfer, and skin humidity. The thickening of the additional skin layer frequently results in a significant modification of the surface morphology, heat transfer, and the corresponding sensation. Thin layers have limited performance in terms

The authors declare no competing interest.

This article is a PNAS Direct Submission.

[1]J.J.K. and S.H. contributed equally to this work.

[2]To whom correspondence may be addressed. Email: someya@ee.t.u-tokyo.ac.jp or oskwon79@kribb.re.kr.

This article contains supporting information online at http://www.pnas.org/lookup/suppl/doi:10.1073/pnas.2200830119/-/DCSupplemental.

Published June 9, 2022.

of antimicrobial duration and speed. The skin coverage of polymer or hydrogel film blocks the transfer of air, moisture, and heat. In addition, the antimicrobial performance is focused on the skin side rather than the external side that affects cross-infection. Voids owing to the stiffness of the film or fiber and morphological differences compared to the skin further limit conformality, heat transfer, and water/air permeability (29).

Here, we propose an antimicrobial skin protection platform copper nanomesh, which prevents cross-infection while minimizing modification of intrinsic skin properties such as interfacial morphology, temperature change rate, and skin humidity. The thin thickness and porous structure of the nanomesh allow conformal attachment to the fingertips, regardless of the mechanical and structural variations of the fingerprints, nails, and interfaces. To impart antimicrobial properties, copper, one of the most well-known antimicrobial (nano)materials (30–33), was coated with maintaining the nanomesh structure (copper nanomesh, from here onward). The measured inactivation rates of copper nanomesh against *Escherichia coli* bacteria and influenza virus A (H1N1) were 99.99% within 1 min and 10 min, respectively. It was found that the nanomesh structure contributed to the acceleration of bacterial inactivation compared to the copper film. Furthermore, it exhibited high biocompatibility with the skin cells and stable antibacterial performance even after long-term use (more than 6 h), including water immersion (more than 1 h).

In addition, we investigated the naturalness of the copper nanomesh compared to that of the copper film and conventional gloves. As confirmed using the artificial skin and fingerprint recognition, the proposed copper nanomesh exhibited a higher conformability compared to that of the copper film. The copper nanomesh showed a high hydrophobicity to block external contaminants in solution while having high gas permeability and maintaining the skin humidity in a safe range. Additionally, the insertion of copper nanomesh did not affect the temperature change rate, which is important to maintain the sensation and comfort fit of the skin. Finally, the copper nanomesh was compared to the glove by wearing on our hands and interacting with various real-life objects. Using the proposed copper nanomesh, we successfully achieved an effective prevention of cross-infection and less-hindered thermal recognition of objects.

Results

On-Skin Attachment and Antibacterial Effect. Fig. 1*A* shows the photographs and magnified structures of the copper nanomesh on a fingertip. Instead of the entire hand, the fingertips were selectively covered and selected as the target of copper nanomeshes because they play a major role in human-object interactions. Microbial transfer and infection from objects to the inner body frequently occur through the contamination of fingertips (34). Despite diverse mechanical and morphological properties of the fingerprints, nails, and nail-skin interfaces, the copper nanomesh was successfully covered without tearing or lifting. This stable wear is owing to the structural advantages of the nanomesh and surface-integrated adhesive nanomesh layer. The structure of the fabricated copper nanomesh is illustrated in *SI Appendix*, Fig. S1. The nanowires were randomly stacked and interconnected with multiple unfilled areas. The directional alignments and densities of nanofibers slightly differed from sample to sample and area to area; however, they demonstrated homogeneity over a large area. The magnified image in Fig. 1*B* presents the conformal and continuous layering of the nanomesh without distorting the intrinsic skin structures. This preservation of skin morphology is highly important for maximally maintaining perceptional resolution (35).

The composition and process from fabrication to adhesion of the copper nanomesh are shown in Fig. 1*C*. After the electrospinning of the polyurethane nanomesh, parylene was coated on each fiber to achieve mechanical stability for successive bending/stretching while maintaining natural body movement (36, 37). On the polymer nanomesh composed of polyurethane/parylene core-shell nanofibers, copper is thermally evaporated only on one side to provide antimicrobial properties with completing the copper nanomesh. In addition, we used biodegradable polyvinyl alcohol (PVA) nanomesh to stably attach copper nanomesh because of its superior adhesion and conformable surface layering onto the skin (38). Using PVA nanomesh increased the maximum adhesion strength between the copper nanomesh and skin by 7.28 times, as shown in *SI Appendix*, Fig. S2. After exposure to the water vapor, the PVA nanomesh was almost dissolved. However, some undissolved components were left and contributed to the adhesion of copper nanomesh to the skin (38).

The scanning electron microscopy (SEM) images are demonstrated in Fig. 1 *D*–*G* to verify the bacterial killing effect and visualize morphological changes in the bacteria. The bactericidal activity of copper nanomesh was evaluated against *E. coli*, representative gram-negative bacterial strains. For that, the parylene-coated polyimide film (125 μm) and polymer parylene-coated polyurethane nanomesh (high density) with and without a 100-nm copper coating were compared (for brevity, we call these a polymer film, polymer nanomesh, copper film, and copper nanomesh, respectively). As shown in Fig. 1 *D* and *F*, bacteria incubated with polymer film or polymer nanomesh had no cell wall disruption of the bacteria and no external ultrastructural changes with regular and typical morphology. Moreover, the cell sizes were uniform, as presented in the existing studies (39). In contrast, there were significant morphological changes in the cells exposed to copper nanomesh, as shown in Fig. 1 *E* and *G*.

The bacteria, incubated with copper nanomesh, showed the formation of pores and pits on the cell membrane. It is well known that the wet condition of bacteria on the copper surface causes the cell membrane and cytoplasm to be damaged (40). In addition, the biofilm stretches until it ruptures in direct contact with the nanostructures of the copper nanomesh (41). After further exposure, the shapes of bacteria on the copper nanomesh became thin, irregular, wrinkled, and coarse, as shown in *SI Appendix*, Fig. S3 (42). These effects were observed within a few seconds of exposing the bacteria to the copper nanomesh, and the morphology of most of the cells changed in the early stage of incubation. Consequently, similar to the copper film, copper nanomesh inhibits bacterial growth and kills them.

Evaluation and Mechanism of Antimicrobial Activities. We compared the antimicrobial efficiencies of different materials and structures to confirm and optimize the bacterial inactivation performance of the copper nanomesh. The *E. coli* concentration was 1×10^6 colony-forming units (CFU)/mL, and the reaction solutions were collected after the exposure to the copper nanomesh for 30, 180, and 600 s. The colony counting method was used to determine the death rate of bacterial cells. After incubation, the number of bacteria observed on the Luria–Bertani (LB) agar plates decreased along with a visible decrease in the viability, as expected. The copper nanomesh exhibited superior performance in inactivating *E. coli* within 1 min, as shown in Fig. 2*A*. Moreover, we compared the

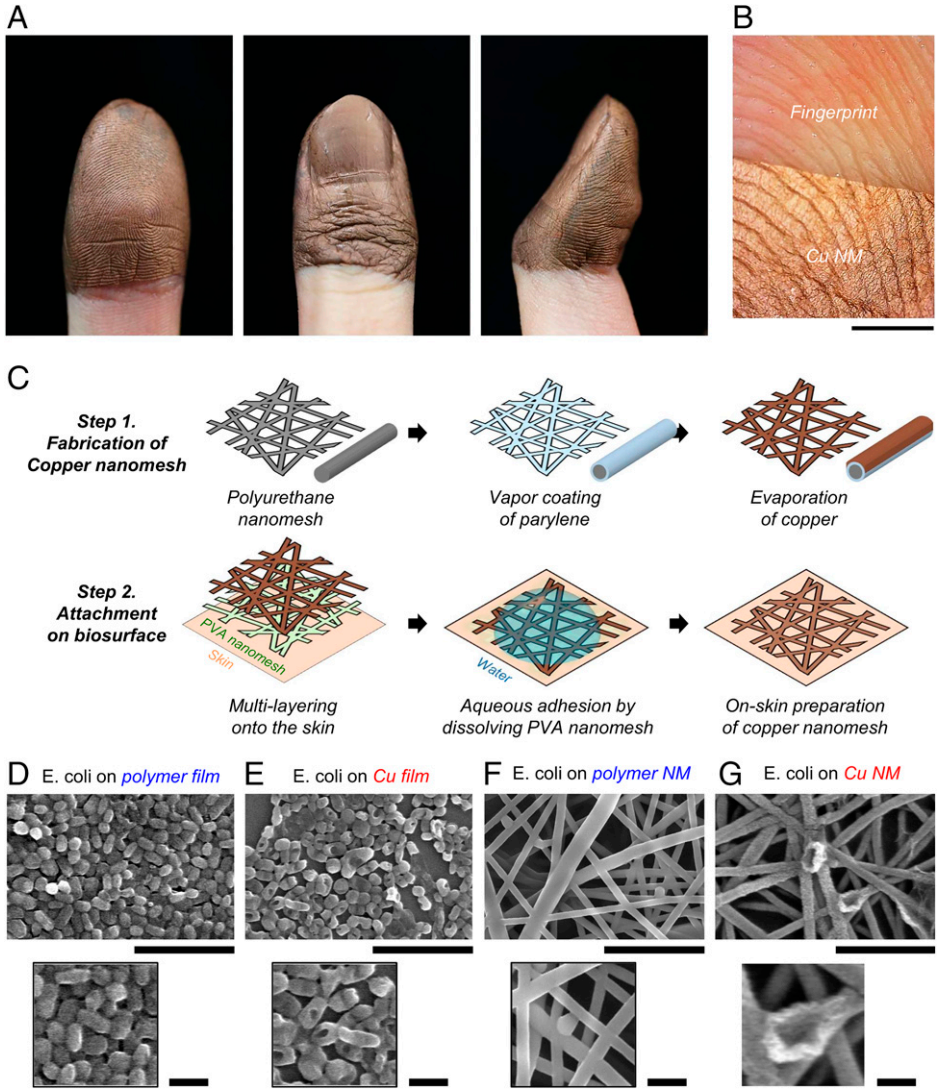

Fig. 1. Optical images of nanomesh on skin and bacteria on different substrates. (*A*) Views of copper nanomesh on a fingertip from different angles of fingerprint, nail, and side. (*B*) Magnified optical image of the copper nanomesh attached to a fingerprint. (Scale bar, 2 mm.) (*C*) Fabrication and attachment process. Step 1. Formation of polyurethane nanomesh by electrospinning, vapor coating of parylene, and thermal evaporation of copper. Step 2. Multilayering of copper nanomesh and PVA nanomesh onto the skin, aqueous adhesion by dissolving PVA nanomesh and drying, and on-skin preparation of copper nanomesh. (*D*–*G*) SEM images of *E. coli* after exposure to each sample for 3 min on the polymer film (*D*), copper film (*E*), polymer nanomesh (*F*), and copper nanomesh (*G*) . Cu, copper; NM, nanomesh. (Scale bars, *Top*, 5 μm; and *Bottom*, 1 μm.)

antimicrobial efficiencies of the proposed copper, gold, and polymer nanomeshes. Fig. 2*B* shows that only the copper nanomesh inactivated the bacterial cells, while no visible inactivation could be observed in other cases. The cell viability ratio dropped below 50% within 30 s after exposure to the copper nanomesh. After being exposed to copper, polymer, gold nanomeshes, and control for 60 s, the viability of *E. coli* was estimated to be 0, 100, 100, and 100%, respectively, as presented in *SI Appendix*, Fig. S4. Moreover, the cell death of *E. coli* occurred only in the case of copper-coated nanomesh, whereas the polymer nanomesh or gold coating did not cause any bacterial inactivation. Therefore, the antimicrobial effect originates from the coated copper, not the underlaid polymer nanomesh or other factors such as external stimuli or drug substances (43–45). Furthermore, the nanofiber densities of copper nanomeshes were varied in the range of low, medium, and high by changing the electrospinning time to determine the optimal structure of the nanomesh (*SI Appendix*, Fig. S5). *E. coli* was exposed to copper nanomesh for 0 to 300 s. After being exposed, it was transferred to an LB agarose gel and subsequently incubated at 37 °C. The cell viability ratios for the copper nanomesh with different densities and copper films are compared and shown in Fig. 2*C* and *SI Appendix*, Fig. S6. The copper nanomesh with high density exhibited the strongest bacterial inactivation within 10 s to 30 s, resulting in death of bacterial cells in the early stage. In the medium and low density copper nanomeshes, the antibacterial effect was shown within 60 s and 180 s, respectively. Bacteria exposed to the copper film showed an antibacterial effect at 300 s and it was the lowest antibacterial effect compared to copper nanomesh. Considering the amount of copper deposited on the surface was higher on the film than on the nanomesh, the higher performance of nanomesh is originated from the nanostructure of copper nanomesh (46).

In addition, influenza virus A (H1N1) was used as the target pathogen to confirm the antiviral feature of the copper nanomesh. The antiviral test was conducted comparably to the antibacterial test. The virus concentration was 1×10^8 PFU/mL, and the sample solutions were collected after being exposed to the copper nanomesh for 5, 10, and 30 min. Fig. 2*D* and *SI Appendix*, Table S1 demonstrate that the plaque of Madin–Darby Canine kidney cells significantly decreased after

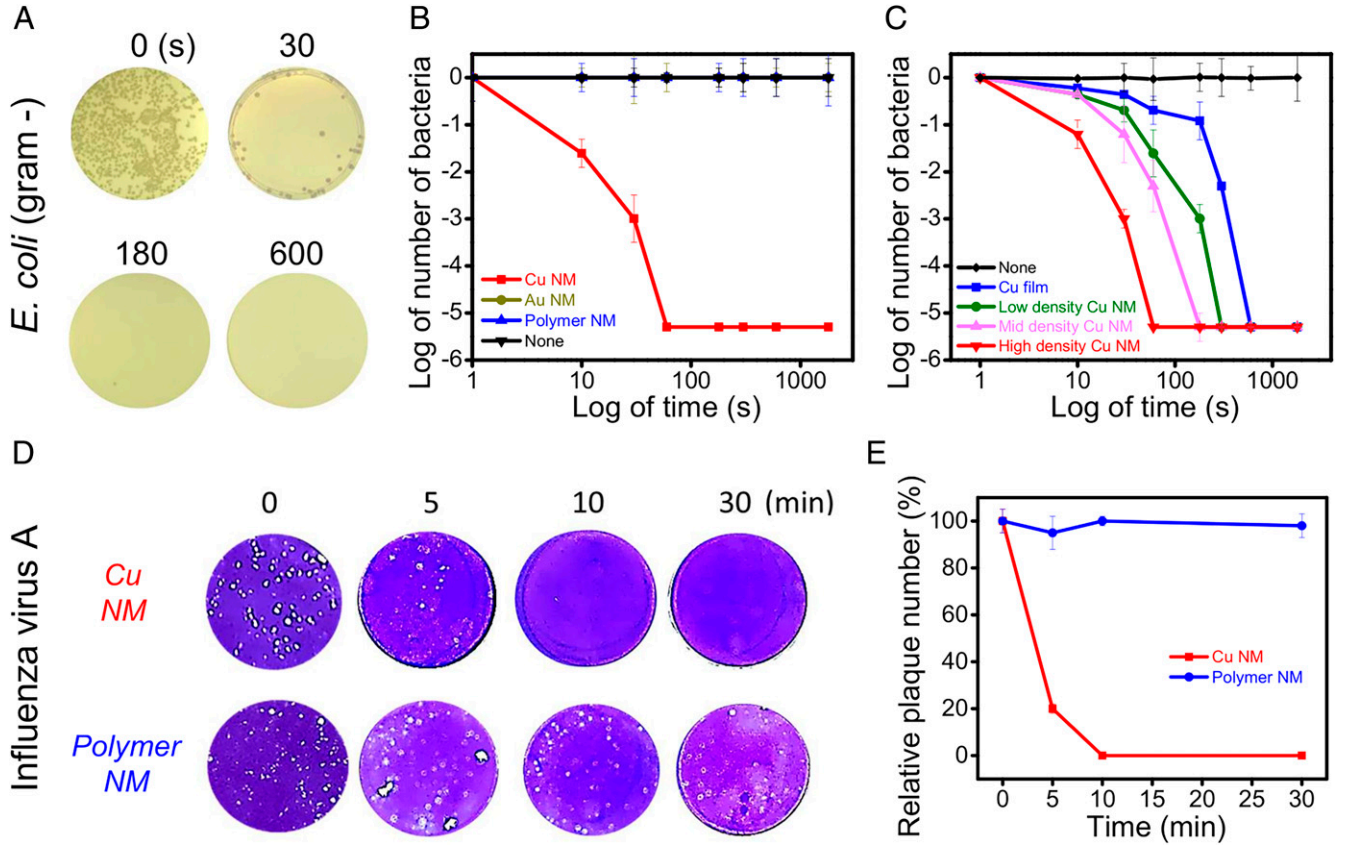

Fig. 2. Microbial inactivation efficacy. (*A*) Colony of *E. coli* upon different exposure times to the copper nanomesh. (*B*) Bacterial viability assay by nanomeshes having different coating materials. (*C*) Bacterial viability assay of copper nanomeshes with different densities and film. (*D*) Plaque assay of influenza virus A (H1N1) upon different reaction times to the copper and polymer nanomeshes. (*E*) Relative plaque number by the copper and polymer nanomeshes. The error bars represent the SD of three independent tests. Au, gold; Cu, copper; NM, nanomesh.

influenza virus A was exposed to the copper nanomesh. The relative plaque numbers are expressed as percentages in Fig. 2*E*. The copper nanomesh effectively inactivated 80% of the viruses within 5 min and 99.99% of the viruses within 10 min. Conversely, the polymer nanomesh showed no reduction of the virus. This explains that copper is the major source of antiviral properties, as in the case of bacteria (47). Based on these superior antiviral properties, the copper nanomesh is expected to be used to inhibit various types of viruses including SARS-CoV-2, as previously reported with the experiment on the copper surface (48, 49). The antimicrobial activity of copper nanomesh can be attributed to the antimicrobial performance of metal nanomaterials, which is copper-coated nanofiber in this research. The bioactivity mechanisms can be due to either the whole metal nanostructure or the metal ion release from the surface and these affect numerous target sites such as cell membranes, membrane-bound proteins, inhibition of enzymatic activity, and nucleic acids (50). The bactericidal activity of these metal nanomaterials depends on their size, stability and concentration added to the growth medium, and the structure also has a significant impact on the destruction of biofilms (17, 51). Metal nanoparticles cause damage by rupturing the cell wall or through the cell membrane, contracting the cytoplasm, and separating the cell membrane. Metal nanoparticles limit bacterial growth by passing through the nanometer pores present in the cell membrane of most bacteria, and additionally, it disrupts important pathways and results in microbial cell death (16, 52). It also involves the formation of reactive oxygen species (ROS) that increase oxidative stress inside microbial cells (50). Furthermore, in the past few years, copper is known for its antimicrobial properties, and it has been demonstrated that it can inactivate various types of viruses such as influenza A, coronavirus (53), HIV type 1 (HIV-1), and unenveloped single or other enveloped or RNA viruses and double-stranded DNA (54). The mechanism of inactivation of viruses is not yet fully understood; however, it is known that the cytoplasmic membrane is severely damaged during the inactivation process (55). Therefore, the copper nanomesh developed in this study has both the antimicrobial effect of copper and the effect of nanomesh as a structure, so it can have an excellent effect as an antibacterial material.

Stabilities, Reusability, and Safety of Copper Nanomesh. We confirmed the aqueous and mechanical stabilities of the copper nanomesh for practical usage in real-life applications. First, for the aqueous stability, we dipped a copper nanomesh coated on the fingertip in the water (*SI Appendix*, Figs. S7, S8 *A* and *B*, and S9 *C* and *D* and Movie S1). After observing the nanomesh on the fingertips during and after the dipping, we were able to confirm the physical/chemical maintenance of copper nanomesh and stable attachments between copper to polymer nanomesh, and copper nanomesh to hand. We think the hydrophobicity of copper nanomesh contributes to this water stability (which will be discussed later). The mechanical stability has been tested by rubbing the copper nanomesh on the fingertips with another fingertip four times (*SI Appendix*, Fig. S9 *A* and *B* and Movie S2) and using hands for 6 h under normal life conditions including typing and grabbing a mouse. Although slight detachment on the edge and a hole in the middle appeared, the overall coverage was maintained without huge detachment. On the other hand,

the nanomesh can be easily and completely removed after usage simply by dipping it in the water and rubbing it. By dissolving PVA nanomesh as an interlayered glue and drying up, the copper nanomesh has strongly adhered to the fingertips. The attachment of copper nanomesh to the fingertip was maintained even after dipping in the water for a long time (*SI Appendix*, Fig. S8 *A* and *B*). However, water immersion weakens the adhesion between the copper nanomesh and skin, so it can be easily removed partially or entirely by rubbing the edges of the nanomesh in water. (*SI Appendix*, Fig. S9 *E* and *F*). Because the adhesive bonding occurs on the water-soluble PVA nanomesh rubbing with water can completely separate the copper nanomesh from the skin (*SI Appendix*, Fig. S9 *G* and *H*). We think this point is important for the reuse and separate collection of metal compounds.

To investigate the reusability of copper nanomesh against successive exposure to pathogens (*SI Appendix*, Figs. S10 and S11), we performed an in vitro test of copper nanomesh to prevent any biological distortion from the skin. In the first use, a 100% antimicrobial effect was induced within 30 s, and in the second and third use, more than 95% of cells were killed within 30 s. In addition, more than 95% of cell death was confirmed within 60 s in the fourth use, and 85% of cell death was confirmed within 600 s in the fifth and sixth use. This result confirms the copper nanomesh as a reusable platform. The decrease in antimicrobial performance might be caused by the occurrence of physical exfoliation and ionic release during reuse or testing in aqueous conditions as demonstrated in other (56, 57).

To evaluate the biocompatibility of copper nanomesh on the skin, cell viability was measured through a cytotoxicity test under aqueous conditions. Skin cells (HaCaT) were exposed to polymer, gold, and copper nanomesh. As shown in *SI Appendix*, Table S2, all samples showed good biocompatibility and low toxicity until several hours after the test. The cell viability rate of copper nanomesh was almost maintained until 3 h (95%) and slightly decreased to 87% and 85% after 6 and 12 h, respectively. Considering all tests are performed in aqueous media, these results show that copper nanomesh is safe enough for use in daily living conditions, which rarely are exposed to moisture for long periods. In summary, we observed significant antimicrobial activity against the bacteria *E. coli* and influenza virus A species, confirming the potential of the copper nanomesh as an antibacterial agent.

Conformality and Fingerprint Recognition. The conformality of the copper nanomesh on the structured surfaces was quantitatively compared to that of a film or glove, as shown in Fig. 3. First, we used artificial skin as the model system because of its structural similarity to real skin. When we compared the surface morphologies using optical imaging, cross-sectional profiling, and histogram counting of the vertical height distribution, as presented in Fig. 3 *A*–*C* and *SI Appendix*, Fig. S12, respectively, the morphological changes in the covering layers were differentiated. In the case of the copper nanomesh, the structure of the artificial skin was approximately maintained with several ridges and valleys. For the comparison, the copper film was prepared by depositing copper on the thinner polymer film. We note that we used 2 μm parylene as the polymer film in this and the following sections for their thinness, instead of 125 μm polyimide film used for the reliable biotest. When the copper film covered the artificial skin, the surface morphology was replaced by irregular cracks and grains. Moreover, it was difficult to find any morphological evidence of underlaid artificial skin in the glove. The results of the numerical analysis before (black) and after the copper nanomesh attachment (red) were highly comparable. Indeed, the copper film and glove yielded completely different surface morphological data. The peaks of the copper film were considerably larger than those of the artificial skin, as shown by the additional peaks in Fig. 3*C* (blue). The surface profile became approximately flat without any noticeable ridges or valleys in the glove (green).

These differences in conformality were demonstrated with the fingerprint, as shown in Fig. 3*D* and *SI Appendix*, Figs. S13 and S14. The optical methods are typically used to acquire the fingerprint pattern images and recognize the fingerprint (58). The fingerprints with and without the copper nanomesh, film, and glove were compared using photo and image processing to evaluate the optical fingerprint recognition performance. The spatial resolution of the fingerprint was maintained on the overall image with clear brightness and contrast differences for the copper nanomesh. However, the edge and some vertical areas in the center exhibited an unfavorable shading owing to the low conformality and high reflection in the case of the film. The glove was principally unable to recognize the fingerprint optically, except in a few areas. Furthermore, fingerprint recognition was evaluated by comparing fingerprint ink images obtained by pressing inked fingerprints with and without different layers on clean paper. Comparable to the previous test, the copper nanomesh maintained its morphology similar to that of the bare fingerprint with a continuous layer, as shown in Fig. 1*B*. However, the area corresponding to the film showed a clear distortion and blur of the fingerprint and the glove sample retained only multiple dots on the glove surface, instead of the fingerprint.

Moreover, we tested the authentication with two electrical devices using the capacitive fingerprint recognition method to evaluate the advantages (*SI Appendix*, Table S3). With conformal and conductive copper nanomesh, the recognition rate was 100% for both devices. However, in the case of the copper film, the recognition rate was dropped to 30 and 10%, and with the glove, the fingerprint was unable to be recognized. The conformal coating of copper nanomesh on the surface can be beneficial for fingerprint recognition compared to the copper film or glove.

Materials and Heat Transfer. We investigated the permeability of water droplets, humidity, and heat to evaluate the interaction between the copper nanomesh and the external environment. Fig. 4*A* and *SI Appendix*, Fig. S15 demonstrate a water droplet on the surface of the copper nanomesh. The hydrophobicity (contact angle of 118.4°) of the copper nanomesh prevents wetting or spreading. The comparison with a droplet on the bare hand confirms that the water-repelling hydrophobicity originates from the copper nanomesh, as shown in *SI Appendix*, Fig. S15. Hydrophobic surface modification is beneficial for preventing microbial skin contamination because microorganisms are frequently cultured in a solution and transported together (59). Also, the hydrophobic surface of copper nanomesh explains the superior water stability and reusability of copper nanomesh.

One of the typical problems with the long-term usage of gloves is eczema. High skin humidity due to moisture and sweat trapped in the glove weakens the skin immune system and causes the growth of bacteria and viruses (60). It has been presented before that the nanomesh with a porous structure exhibits water permeability and enables long-term wear without inflammation (38). However, the actual humidity on the skin with nanomesh had never been measured and compared with

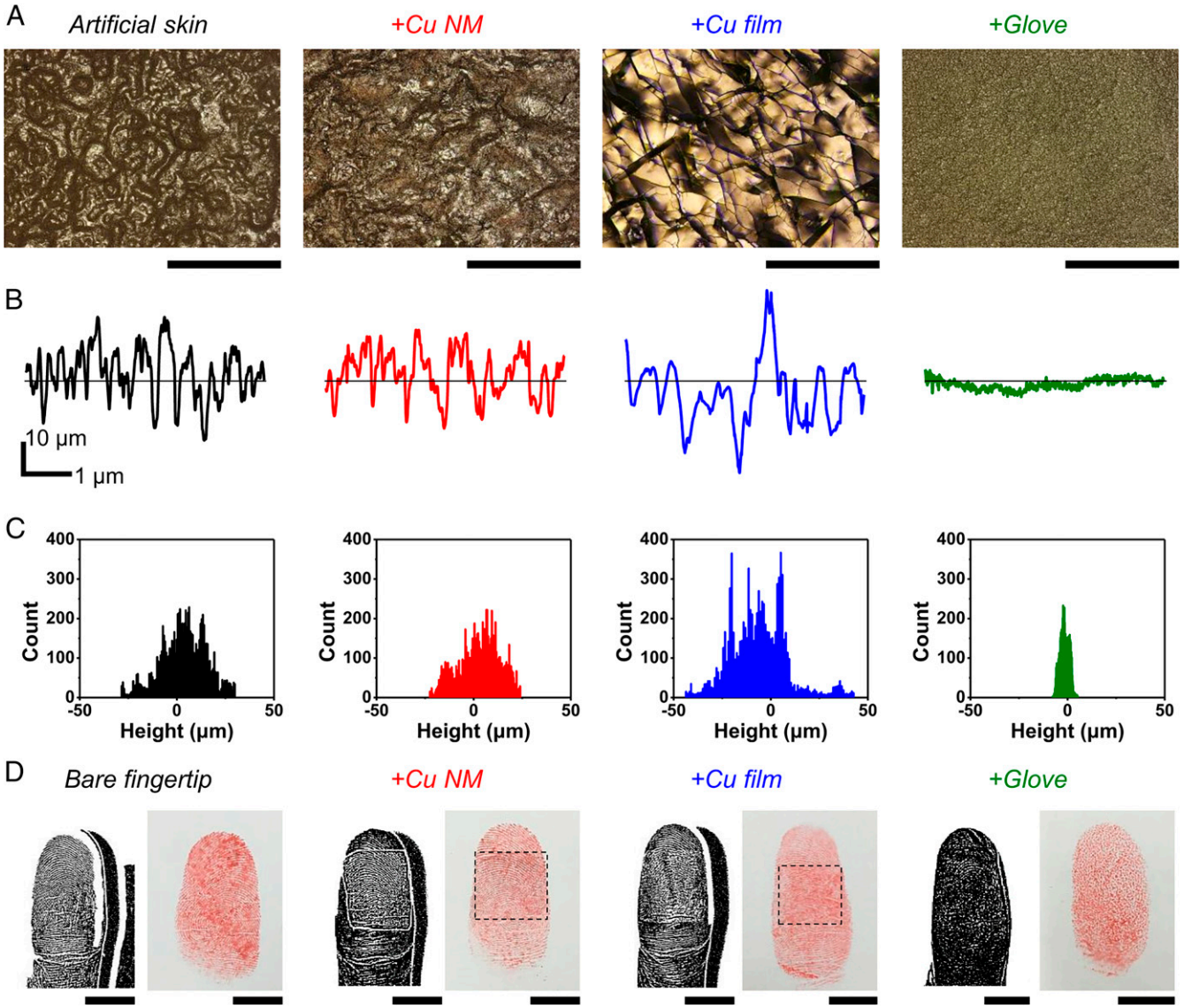

Fig. 3. Conformality comparison. (*A*) Optical images of an artificial skin without and with the copper nanomesh, copper film, and glove (Scale bar, 0.5 mm). (*B*) Surface height profile of each sample. (*C*) Height distribution histogram of *B*. (*D*) Optical (*Left*) and mechanically transferred (*Right*) patterns of a bare fingerprint without and with the copper nanomesh, copper film, and glove. The areas with the copper nanomesh and film are marked with a dotted line. (Scale bar, 1 cm.)

the filmed coverages. Fig. 4*B* shows the measured humidity with and without different coverages on the skin. In the case of the copper film and glove continuously covering the entire skin, the skin humidity showed an immediate increase, which was saturated at high humidity. The humidity of the copper film reached 61, 71, and 80% within 10, 50, and 260 s, respectively, and saturated to ∼81%. The humidity of the glove reached 62, 71, and 80% within 30, 70, and 200 s, respectively, and saturated to ∼88%. Although the humidity with the copper nanomesh was slightly higher (∼54%) than the bare skin (∼46%), both were maintained within the ideal skin humidity range without a significant increase. Using the copper nanomesh allows the vaporization of the sweat underneath, while homeostasis of the skin humidity could be maintained.

Another significant drawback of covering the skin with a layer is the disturbance of the thermal sensation. Our skin feels and differentiates between the materials based on the rate of temperature change (61). For example, when we touch a material, such as wood at room temperature, the cooling rate of our skin is extremely low, and we perceive it as a warm object. In contrast, we perceive metal objects as cold because the cooling rate of our skin is relatively high. Therefore, we compared the interfacial temperature change rates (heating rates) by contacting a hot plate with and without the covering layers, as presented in Fig. 4*C* and *D*, and *SI Appendix*, Fig. S16. When a polymer or copper nanomesh was inserted, the speed of temperature increase rose slightly compared to that without any interlayer on the thermal sensor (2.75 to 2.87 and 2.82 °C/s). Thin polymer films (2 μm) with and without 100 nm copper decreased the heating rate (to 2.51 and 2.61 °C/s, respectively) and the glove resulted in a decrease in the heating rate to less than half (1.28 °C/s) of other samples. This trend was maintained in the cooling experiment performed by contacting different materials, as demonstrated in *SI Appendix*, Figs. S17 and S18 and Table S4. The insertion of copper nanomesh or film slightly decreased the cooling rate, and the glove showed a noticeable decrease. Considering that the difference in the rate of temperature change is used for material recognition, the overall decrease in the rate of temperature change with the glove can result in an inadequate thermal sensation of materials.

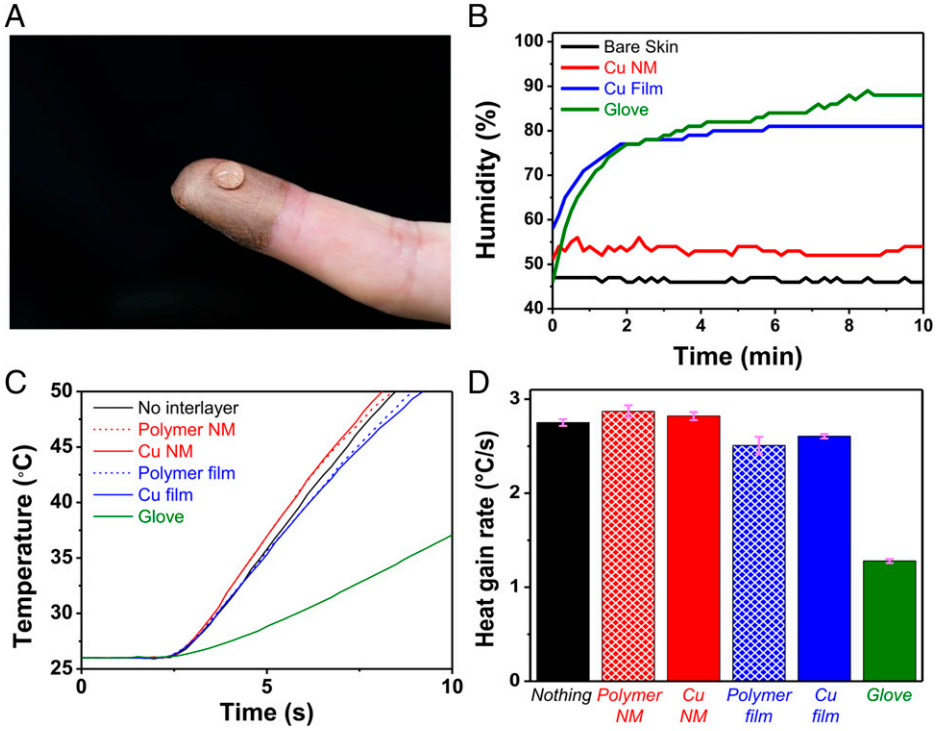

Fig. 4. Selective transportability of matter and heat. (*A*) A droplet placed on the copper nanomesh coated on a fingertip. (*B*) Skin humidity as a function of the wearing time with different coverages. (*C*) Measured temperature as a function of the contacting time with different interlayers between. (*D*) The rates of heat gain were compared as the interlayer. The error bars represent the SD of five independent tests.

Moreover, the copper nanomesh or film is expected to deliver the thermal sensation of materials at a level similar to that of the bare hand without any covering layer.

The selective transfer of heat and materials through the copper nanomesh is shown in *SI Appendix*, Fig. S19. Surface hydrophobicity repels water droplets that can contain microbes. In contrast, the inner sweat can be vaporized and removed through the pores of the copper nanomesh, while preserving the skin humidity equilibrium. Thin and highly conformal nanomesh coated with copper, one of the most thermally conductive materials, conveys heat, which can lead to a proper thermal sensation. Due to the advantageous mesh structure (62), the transport of water, air, and heat was enabled without a huge change from the bare skin. Additionally, we have previously demonstrated that the metal-coated nanomesh preserves the pressure sensing of the skin without any disturbance or distortion (63). These results confirm that our copper nanomesh can be used for long-term skin protection while maintaining skin conditions and functionality.

On-Skin Application and Comparison with Gloves. We investigated the prevention of cross-infection and compared the amount of thermal transfer change with a glove (Fig. 5) to demonstrate the advantages of the presented copper nanomesh in real-life applications. The risk of cross-infection in real life is a critical public health concern, particularly during times of epidemic threat (64). Some bacteria and viruses are known to be able to survive and spread freely without a host for a certain amount of time (49, 65). Therefore, the effect of indirectly transmitted microbes on disease progression is important for microbial infection control purposes. To this end, we conducted a study on the cross-infection between people and objects with *E. coli* bacteria. We first hypothesized the following primary and secondary infections: the primary infection is the transfer of bacteria to the skin when grabbing an object infected with bacteria, and cross-infection occurs when the bacteria transferred to the skin come into contact with other objects (66). Therefore, we designed and conducted a test to investigate if the antibacterial copper nanomesh can prevent cross-infection. For this test, we chose six representative products with different compositions, structures, and interactions with the hand, such as a stainless-steel spoon, plastic mouse, glass bottle, cotton fabric, paper post-it, and plastic syringe. Then we contaminated six objects with the bacteria and prepared copper nanomesh-coated second skin and normal gloves.

The *Top* part in Fig. 5*A* is the result of using a second skin with the copper nanomesh, and the *Bottom* part is achieved using gloves in a laboratory or hospital to prevent direct infection of the human skin. The initial bacterial concentration on the object was 1×10^6 CFU/mL, and based on previous experiments, we grabbed an object and held it for up to 300 s under constant pressure. The surviving populations of all tested bacteria decreased significantly in the copper nanomesh, unlike gloves that exhibited bacterial growth. Bacteria were reduced on the copper nanomesh by 50% or more within 3 min, and all were eliminated within 5 min, as presented in *SI Appendix*, Fig. S20. However, the number of bacteria was maintained at 100% even after 5 min of exposure in the case of the conventional glove. Consequently, the use of copper nanomesh as the second skin can protect against secondary infection from contact with real objects that can be easily contaminated by microorganisms (30).

Additionally, we compared the relative disturbance of thermal interactions by grabbing different objects with copper nanomeshes and gloves. A thin-wire thermocouple was placed on the fingertip to monitor the temperature change during the contact process. When an object at room temperature was touched, the temperature was changed from body temperature

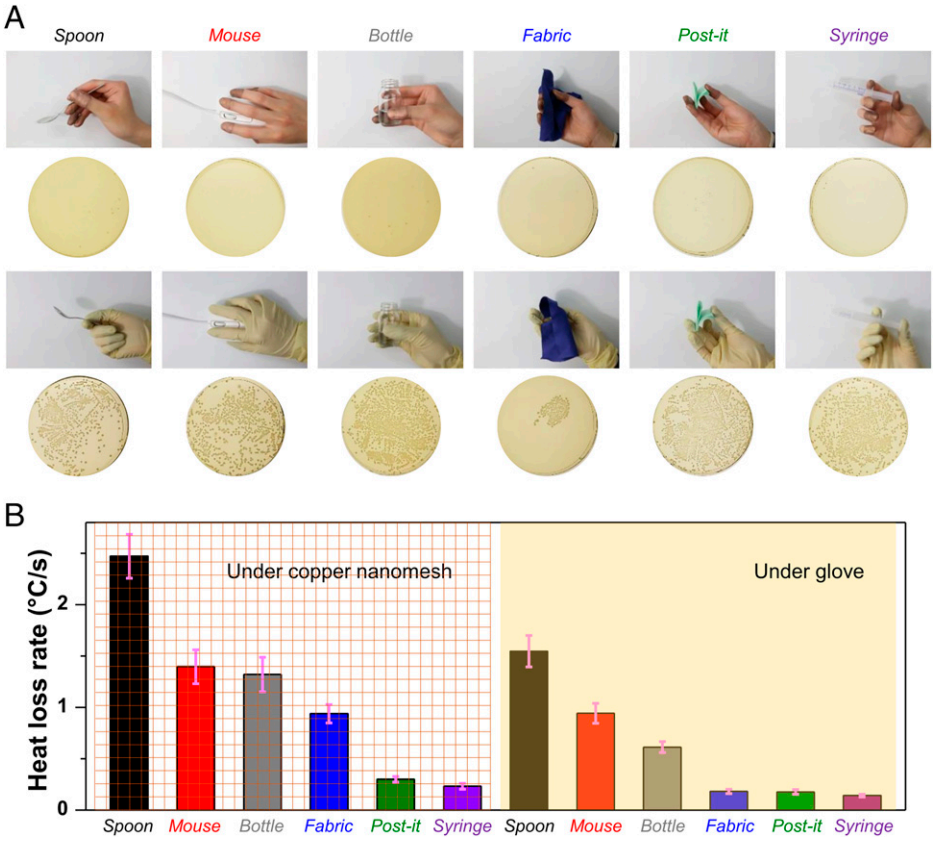

Fig. 5. On-hand usage demonstration. (*A*) Photographs of holding different objects with a copper nanomesh and glove. The corresponding bacterial culture plates of *E. coli* after cross-infection are placed below. (*B*) Heat loss rate comparison by touching different objects at room temperature with a copper nanomesh or glove on the hand. The error bars represent the SD of three independent tests.

(~36 °C) to room temperature (~26 °C) with different heat loss rates. Although both the object and covering worn affect the body temperature change during contact, the two cannot be differentiated as mimicked in our experimental setup. As shown in Fig. 5*B*, different objects touched with the fingertip wearing copper nanomesh showed different heat loss rates in the range of 0.23 to 2.47 °C/s. Moreover, the range was decreased from 0.14 to 1.55 °C/s in the case of the glove on the fingertip, making object identification more difficult. In particular, the heat loss rates with the glove for the metal spoon, plastic mouse, glass bottle, plastic fabric, paper post-it, and plastic syringe decreased to 62.6, 67.5, 45.4, 19.5, 59.1, and 60.9% of that with the copper nanomesh. The significant decrease in the heat loss rate of the plastic fabric can be attributed to its softness; however, further investigations are required. The thermal distortion caused by the wearing device disturbs the proper recognition of objects. That is, if we are wearing gloves, it is difficult to differentiate metals, which provide us with a cool sensation, and wood, which provides us with a warm sense, unless we are wearing a special glove that gives thermal feedback with an ultrafast temperature change rate (2.75 °C/s) (67). Hence, the copper nanomesh outperformed the glove in the thermal identification of objects.

Discussion

In this study, we fabricated a copper nanomesh and demonstrated its antimicrobial properties and preservation of skin naturalness with conformality, thermal conductivity, and skin humidity. The antimicrobial properties of copper were confirmed using the bacterial and viral inactivation tests, while further enhancement of the large surface area of nanomesh was demonstrated. The prevention of cross-infection was tested with a copper nanomesh by placing on the hand and interacting with various objects. The thin and porous nanomesh structure provided ideal compatibility with the skin functions. In addition, the proposed copper nanomesh exhibited advances in thermal transfer with a positive potential in thermal sensation and object identification.

For the commercial application of the proposed copper nanomesh as an alternative to gloves or other skin protective wear, there are a few issues remaining to be addressed. In this study, we chose thermally evaporated copper as the antimicrobial material, but it can be substituted by other antimicrobial materials such as silver or other organic compounds according to the use. The size and density of the nanomesh can be further optimized, and the covered area can be expanded to the entire hand or other body parts. In addition, more systematic studies on the mechanical and chemical stabilities in the long term are required to broaden the scope of the application. Consequently, this study introduces an antimicrobial platform to combat infectious diseases that threaten humans, particularly in the event of a pandemic, and it is expected to be advanced toward practical use.

Materials and Methods

Fabrication of the Nanomesh. The fabrication process of copper nanomesh and adhesive PVA nanomesh is shown in previous reports (38). A polyurethane solution for the electrospinning was prepared by diluting the purchased

polyurethane solution (Rezamin M-8115LP, Dainichiseika) to form a 15 wt. % solution with a 7:3 ratio of a mixed solvent of N,N-dimethylformamide and methyl ethyl ketone. The PVA solution was prepared by dissolving PVA powder (EG-22P, Nippon Synthetic Chemical Industries) into distilled water with 10 wt. %. The solutions became transparent after the complete mixing by stirring for more than 3 h. The electrospinning (NANON-03, Mecc Corp.) was performed at room temperature (~26 °C) with about 40% humidity maintenance. The solutions were electrospun from a plastic syringe with a metallic needle (18G) of 15 mm to the silicone-coated paper substrate (cooking sheet, Toyoalumi). The applied voltage was 20 kV with a tip-to-substrate distance of 15 cm. The flow rate was 0.6 mL/h, and the length and diameter of the rotating drum were 20 and 20 cm, respectively. The densities of the nanomesh were controlled by the coating time. The densities of polymer and copper nanomeshes (5 min for the low, 10 min for the mid, and 20 min for the high) are chosen based on the flexibility and breathability as demonstrated in our previous reports (36, 63). Based on the highest performance in Fig. 2*C*, a high density of 20 min was used for the other tests. In the case of PVA nanomesh, the spinning time was fixed to 1 h to make the densely packed adhesive layer. After the electrospinning, the nanofiber was moved to the polyimide frame (125-μm thickness) for better handling and to prevent any deformation. For better mechanical stability and biocompatibility, 200-nm parylene (diX-SR, Daisan Kasei) was coated (PDS2010, Specialty Coating Systems) conformally, especially to strengthen the joint between nanofibers. The 100-nm-thick copper and gold were coated using the thermal evaporator (VPC-260F, Ulvac Kiko. Inc. and Ex-200, Ulvac Kiko. Inc.) at a pressure lower than 10^{-2} Pa. During the deposition process of parylene and metal, 125-μm polyimide film was used as the frame of the nanomesh for ease of handling. After the fabrication, all nanomeshes were preserved under ambient conditions.

Fabrication of the Thin Film. For this research, two kinds of polymer films were used as themselves and with the copper deposition. Thick polymer films were prepared for reliable antibacterial testing without tearing or folding the polymer film by sequentially coating 200-nm parylene and 100-nm copper on 125-μm polyimide films. All coating processes were carried out simultaneously with copper nanomesh. For other tests including conformality and transportation, 2-μm parylene film was fabricated and used as a substrate by spin coating of the fluorinated polymer (1:6 volume ratio of Novec 1700 and 7100, 3M) at 2,000 rpm for 30 s as a sacrificial layer on the top of 125-μm polyimide film and the following parylene deposition. The samples were transferred to the frame made of 125-μm polyimide film for ease of handling.

Morphological Characterization. The optical images of copper nanomesh on fingertips were taken with a digital camera (Nikon). The magnified image of copper nanomesh on the fingerprint was obtained using the mobile USB microscope (AD4113TS, Dino-Lite). For the optical images on the artificial skin (Bioskin plate, Beaulax), the color three-dimensional laser microscope (VK-9710, Keyence) was used. To prevent any structural or chemical modification, we just used the artificial skin as purchased. For the glove, a typical latex experimental glove (8-4053-01 Kualatec Gloves, As One Corporation) with thicknesses of 160 μm for the palm and 190 μm for the fingertips was used. The cross-sectional profile was measured with a profilometer (Dektak-XTA, Bruker) and analyzed with the software (Vision64, Bruker). For SEM, two kinds of equipment were used for the morphological investigation of nanomeshes (S4800, Hitachi High Technologies) and with bacteria on them (Sirion, FEI) without any metal coating.

Physical Characterization. The contact angle was measured with the equipment (DM-CE1 Contact Angle Meter, Kyowa) and automatically calculated with the software (FAMAS, Kyowa Interface Science Co.). The slide glass was used as a substrate. The measurement was performed at room temperature (~26 °C), and the volume of the water droplet was 0.5 μL. The adhesion force was recorded using the tensile tester (AG-X, Shimadzu) by attaching one end of the nanomesh to the 125-μm polyimide film for uniform holding and pulling. On the other end, a part of the nanomesh (1.5 cm × 0.5 cm) was attached to the skin by dissolving the PVA nanomesh. The size of the entire nanomesh was 1.5 cm × 1.5 cm and the lifting speed was 10 mm/min.

Thermal Characterizations. The temperature was measured with a thermocouple and a digital multimeter (34465A, Keysight) with the software (BenchVue, Keysight) every 0.2 s. Enough resting time was waited for the thermal equilibrium without huge fluctuation before and between measurements. For the measurements of heating and cooling rates, the slopes of the first 3 s of the attachment/detachment to/from the hot plate were used. The starting temperature was fixed to the room temperature of equilibrium (~26 °C). To minimize the distortion from a contact, the thermocouple was attached between the neodymium-magnet and the hot plate having a magnetic top. Each film and nanomesh was inserted between two flat magnets to minimize the effect of the contacting area size and roughness. Each measurement was done more than five times. The equivalent tests of five different samples were repeated for reproducibility, and the SD values appeared as the error bars.

On-Skin Characterizations. For the skin attachment, PVA nanomesh was used as previously explained. After it was placed onto the skin, ethanol was applied for the conformal coating and exposed to the water vapor for the dissolution of PVA and attachment. The size of PVA nanomesh was bigger than the attached copper nanomesh to ensure sufficient adhesion. The fingerprint was measured by taking the photo, analyzing it with the software (Fingerprint Photographer, Muskaan Diamonds Inc.), stamping it on the ink pad, and pressing it on white paper for 5 s each. The fingerprint recognition was performed by contacting the finger with and without wearing different substrates on the skin onto the digital devices (device 1, iPhone X, Apple and device 2, iPad 10.2, Apple) and unlocking them. The humidity on the skin was measured by attaching a humidity sensor (CL-M53R, Shinyei) and covering it with nanomesh, film, and gloves. The covered area was 1.5 cm × 1.5 cm, and the measurement was performed immediately after the attachment. The temperature was measured by fixing the thermocouple on the skin and covering it with different nanomeshes or gloves. If necessary, the liquid bandage (Medi-Shield, Kobayashi) was used to fix the wiring to the skin. For the comparison of the temperature decrease rates of different objects on the skin, we used a prepared spoon (steel), mouse (plastic), bottle (glass), fabric (cotton), post-it (paper), and syringe (polypropylene). Each item was naturally grabbed with the finger equipped with the temperature sensor and covered with a nanomesh or glove. For the skin test, the study protocol was thoroughly reviewed and approved by the ethical committee of The University of Tokyo (approval no. KE19-32), and informed consent was obtained from all participants for all experiments. The equivalent tests of five different samples were repeated for reproducibility, and the SD values appeared as the error bars.

Antimicrobial Performance of Copper Nanomesh. Gram-negative bacterium *Escherichia coli* was grown in LB media at 37 °C under shaking (150 rpm) and then the bacterial concentration was adjusted to 1×10^6 CFU/mL. *E. coli* was exposed to various material-embedded polymer layers (polymer, plutonium, copper, gold) and various concentrations of copper nanomesh. These samples were incubated at 37 °C, and then 50 μL of bacteria was acquired at each time interval. In addition, the samples were prepared onto the LB agar plate at 37 °C overnight for antimicrobial test and confirmed the number of surviving bacteria was collected by bacterial colonies counting.

The influenza virus of 1×10^8 PFU/mL was incubated with copper nanomesh and polymer nanomesh at 37 °C. Then, each 50 μL of the sample was collected for plaque assay on Madin-Darby canine kidney (MDCK) cells, and the plate was maintained at 37 °C in 5% CO_2 until plaques were visible. For the plaque assay, MDCK cells in 6-well plates were infected and incubated for 30 min at room temperature. The inoculum was removed and cells overlaid (1% agarose, 1 μg/mL N-tosyl-L-phenylalaninyl-chloromethylketone), and then the cells were incubated at 37 °C and 5% CO_2 for 72 h. Viral plaques were counted after 3 d of incubation at 37 °C in a CO_2 incubator. The equivalent tests of three different samples were repeated for reproducibility, and the SD values appeared as the error bars.

Aqueous and Mechanical Stabilities and Reusability of Copper Nanomesh. For the tests of aqueous and mechanical stability, the copper nanomesh was placed on the skin and completely dried under ambient conditions for proper attachment to the skin. The aqueous test was confirmed by dipping a fingertip under distilled water and taken out after a few seconds (*SI Appendix*, Figs. S7 and S9 *C* and *D* and Movie S1) or 5 min (*SI Appendix*, Fig. S8). For the mechanical stability test, the copper nanomesh on the fingertips was rubbed on another fingertip four times (*SI Appendix*, Movie S2) and used for 6 h under normal life conditions including typing and grabbing a mouse. For the complete

detachment after the usage, the copper nanomesh was dipped into the water and gently rubbed with another finger (*SI Appendix*, Movie S3).

To investigate the reusability of copper nanomesh against successive exposure to pathogens (*SI Appendix*, Figs. S10 and S11), we performed an in vitro test of copper nanomesh to prevent any biological distortion from the skin. For the first efficacy test of the nanomesh, we exposed 1×10^6 cells to the copper nanomesh for up to 600 s, then immediately transferred them to LB agarose gel, and subsequently incubated them under standard conditions. For the second and followed efficacy tests, we collected the firstly used nanomesh after removing the remained materials in the first test nanomesh by rinsing them with distilled water. After drying in the ambient condition, it was tested under the same conditions as the first. Through a total of six verifications, it was confirmed that the reuse of four times as effective (*SI Appendix*, Figs. S10 and S11).

Toxicity Test. Skin cells (HaCaT) were seeded at an initial density of 1×10^5 cells per well and incubated at 37 °C with 5% CO_2 for 24 h and the pH was maintained at 7.4 to ~8 using Dulbecco's modified eagle medium with 10% fetal bovine serum (FBS) (68–70). Then, they were exposed with copper nanomesh for 0.5, 1, 3, 6, and 12 h respectively, and the cell culture medium was removed and added fresh media. After 24 h, cell viability as an indicator for cytotoxicity was determined by 3-(4,5-dimethylthiazol-2-yl)-2,5-diphenyl-2H-tetrazolium bromide (MTT) assay.

Cross-Infection Test. The copper nanomesh was transferred onto the five fingertips on a hand as shown previously. We prepared a spoon (steel), mouse (plastic), bottle (glass), fabric (cotton), post-it (paper), and syringe (polypropylene) to test the antibacterial effect on different materials. Before experiments, copper-nanomesh-coated second skin and normal gloves were confirmed to be free from the bacteria by the control test. First, 100 μL of bacteria of 1×10^6 CFU/mL was dropped onto the prepared materials, causing contamination. Then, the suspension sample was exposed using the second skin and gloves for up to 5 min. The samples were collected at 1 min, 3 min, and 5 min and then spread to an LB agar plate. Samples were incubated overnight at 37 °C, and bacterial inactivation by the second skin was confirmed by colony counting.

Data Availability. All study data are included in the article and/or supporting information.

ACKNOWLEDGMENTS. We appreciate Sungho Yoo for the helpful discussion and advice. This work was financially supported by the Japan Science and Technology Agency Accelerated Innovation Research Initiative (Grant No. JPMJMI17F1). J.J.K. and C.W., the International Research Fellows of Japan Society for the Promotion of Science, acknowledge the support from the Japan Society for the Promotion of Science (JSPS) Postdoctoral Fellowships for Research in Japan. S.H., L.K., and O.S.K. acknowledge the Research Program to Solve Urgent Safety Issues of the National Research Foundation of Korea (NRF) funded by the Korean government (Ministry of Science and ICT [MSIT]) (NRF-2020M3E9A1111636), Korea Research Institute of Bioscience and Biotechnology (KRIBB) Research Initiative Program (1711134045), Korea Institute of Planning and Evaluation for Technology in Food, Agriculture and Forestry (IPET), and Korea Smart Farm R&D Foundation (KosFarm) through Smart Farm Innovation Technology Development Program, funded by Ministry of Agriculture, Food and Rural Affairs (MAFRA) and MSIT, Rural Development Administration (RDA) (421020-03).

Author affiliations: [a]Department of Electrical Engineering and Information Systems, The University of Tokyo, Bunkyo-Ku, Tokyo 113-8656, Japan; [b]Infectious Disease Research Center, Korea Research Institute of Bioscience and Biotechnology (KRIBB), Daejeon 34141, South Korea; [c]Center for Emergent Matter Science & Thin-Film Device Laboratory RIKEN 2-1 Hirosawa, Wako, Saitama 351-0198, Japan; and [d]Department of Nanobiotechnology, Korea University of Science and Technology (UST), Daejeon 34141, South Korea

Author contributions: J.J.K. and S.H. designed research; J.J.K., S.H., L.K., Y.K., Y.W., C.O., H.W., C.W., K.F., S.L., T.Y., O.S.K., and T.S. performed research; J.J.K., S.H., L.K., Y.K., Y.W., C.O., H.W., C.W., K.F., S.L., T.Y., O.S.K., and T.S. analyzed data; and J.J.K., S.H., S.L., T.Y., and T.S. wrote the paper.

1. J. Lee *et al.*, Thermally controlled, active imperceptible artificial skin in visible-to-infrared range. *Adv. Funct. Mater.* **30**, 2003328 (2020).
2. J. J. Kim *et al.*, Skin electronics: Next-generation device platform for virtual and augmented reality. *Adv. Funct. Mater.* **31**, 2009602 (2021).
3. M. Kaltenbrunner *et al.*, An ultra-lightweight design for imperceptible plastic electronics. *Nature* **499**, 458–463 (2013).
4. D.-H. Kim *et al.*, Epidermal electronics. *Science* **333**, 838–843 (2011).
5. C. Archer, "Functions of the skin" in *Rook's Textbook of Dermatology, Volume 1* (Blackwell Publishing Ltd., Hoboken, NJ, 2010), pp. 1–11.
6. W. Montagna, *The Structure and Function of Skin* (Elsevier, 2012).
7. T. Someya *et al.*, A large-area, flexible pressure sensor matrix with organic field-effect transistors for artificial skin applications. *Proc. Natl. Acad. Sci. U. S. A.* **101**, 9966–9970 (2004).
8. T. Someya *et al.*, Conformable, flexible, large-area networks of pressure and thermal sensors with organic transistor active matrixes. *Proc. Natl. Acad. Sci. U. S. A.* **102**, 12321–12325 (2005).
9. D. J. Lipomi *et al.*, Skin-like pressure and strain sensors based on transparent elastic films of carbon nanotubes. *Nat. Nanotechnol.* **6**, 788–792 (2011).
10. E. Kamalha, Y. Zeng, J. I. Mwasiagi, S. Kyatuheire, The comfort dimension; a review of perception in clothing. *J. Sens. Stud.* **28**, 423–444 (2013).
11. B. Allegranzi, D. Pittet, Role of hand hygiene in healthcare-associated infection prevention. *J. Hosp. Infect.* **73**, 305–315 (2009).
12. A. Bhalla *et al.*, Acquisition of nosocomial pathogens on hands after contact with environmental surfaces near hospitalized patients. *Infect. Control Hosp. Epidemiol.* **25**, 164–167 (2004).
13. S. Andra, S. K. Balu, J. Jeevanandam, M. Muthalagu, Emerging nanomaterials for antibacterial textile fabrication. *Naunyn Schmiedebergs Arch. Pharmacol.* **394**, 1355–1382 (2021).
14. E. O. Ogunsona, R. Muthuraj, E. Ojogbo, O. Valerio, T. H. Mekonnen, Engineered nanomaterials for antimicrobial applications: A review. *Appl. Mater. Today* **18**, 100473 (2020).
15. M. I. Ahamed, R. Prasad, *Advanced Antimicrobial Materials and Applications* (Springer, 2021).
16. A. Baranwal *et al.*, Prospects of nanostructure materials and their composites as antimicrobial agents. *Front. Microbiol.* **9**, 422 (2018).
17. L. Wang, C. Hu, L. Shao, The antimicrobial activity of nanoparticles: Present situation and prospects for the future. *Int. J. Nanomedicine* **12**, 1227–1249 (2017).
18. R. F. Rose, P. Lyons, H. Horne, S. Mark Wilkinson, A review of the materials and allergens in protective gloves. *Contact Dermat.* **61**, 129–137 (2009).
19. B. Arman Amani, S. Bagheri, S. B. A. Hamid, Progress on antimicrobial surgical gloves: A review. *Rubber Chem. Technol.* **89**, 117–125 (2015).
20. Y. Li, P. Leung, L. Yao, Q. W. Song, E. Newton, Antimicrobial effect of surgical masks coated with nanoparticles. *J. Hosp. Infect.* **62**, 58–63 (2006).
21. M. H. Chua *et al.*, Face masks in the new COVID-19 normal: Materials, testing, and perspectives. *Research* **2020**, 7286735 (2020).
22. D. Simões *et al.*, Recent advances on antimicrobial wound dressing: A review. *Eur. J. Pharm. Biopharm.* **127**, 130–141 (2018).
23. S. M. O'Meara, N. A. Cullum, M. Majid, T. A. Sheldon, Systematic review of antimicrobial agents used for chronic wounds. *Br. J. Surg.* **88**, 4–21 (2001).
24. Z. Li *et al.*, Ag nanoparticle-ZnO nanowire hybrid nanostructures as enhanced and robust antimicrobial textiles via a green chemical approach. *Nanotechnology* **25**, 145702 (2014).
25. X. Peng *et al.*, A breathable, biodegradable, antibacterial, and self-powered electronic skin based on all-nanofiber triboelectric nanogenerators. *Sci. Adv.* **6**, eaba9624 (2020).
26. Y. Zhong *et al.*, Antimicrobial/biocompatible hydrogels dual-reinforced by cellulose as ultrastretchable and rapid self-healing wound dressing. *Biomacromolecules* **22**, 1654–1663 (2021).
27. G. Singh *et al.*, Gelatin-based highly stretchable, self-healing, conducting, multiadhesive, and antimicrobial ionogels embedded with Ag2O nanoparticles. *ACS Sustain. Chem.& Eng.* **5**, 6568–6577 (2017).
28. Z. Yang *et al.*, Highly stretchable, adhesive, biocompatible, and antibacterial hydrogel dressings for wound healing. *Adv. Sci. (Weinh.)* **8**, 2003627 (2021).
29. T. Drabek, C. D. Boucek, C. W. Buffington, Wearing the wrong size latex surgical gloves impairs manual dexterity. *J. Occup. Environ. Hyg.* **7**, 152–155 (2010).
30. M. Raffi *et al.*, Investigations into the antibacterial behavior of copper nanoparticles against Escherichia coli. *Ann. Microbiol.* **60**, 75–80 (2010).
31. D. Longano, N. Ditaranto, L. Sabbatini, L. Torsi, N. Cioffi, "Synthesis and antimicrobial activity of copper nanomaterials" in *Nano-antimicrobials* (Springer, 2012), pp. 85–117.
32. C. Sun *et al.*, Durable and washable antibacterial copper nanoparticles bridged by surface grafting polymer brushes on cotton and polymeric materials. *J. Nanomater.* **2018**, 6546193 (2018).
33. J. J. Ahire, M. Hattingh, D. P. Neveling, L. M. Dicks, Copper-containing anti-biofilm nanofiber scaffolds as a wound dressing material. *PLoS One* **11**, e0152755 (2016).
34. P. Rusin, S. Maxwell, C. Gerba, Comparative surface-to-hand and fingertip-to-mouth transfer efficiency of gram-positive bacteria, gram-negative bacteria, and phage. *J. Appl. Microbiol.* **93**, 585–592 (2002).
35. E. Jarocka, J. A. Pruszynski, R. S. Johansson, Human touch receptors are sensitive to spatial details on the scale of single fingerprint ridges. *J. Neurosci.* **41**, 3622–3634 (2021).
36. S. Lee *et al.*, Ultrasoft electronics to monitor dynamically pulsing cardiomyocytes. *Nat. Nanotechnol.* **14**, 156–160 (2019).
37. Y. Wang *et al.*, A durable nanomesh on-skin strain gauge for natural skin motion monitoring with minimum mechanical constraints. *Sci. Adv.* **6**, eabb7043 (2020).
38. A. Miyamoto *et al.*, Inflammation-free, gas-permeable, lightweight, stretchable on-skin electronics with nanomeshes. *Nat. Nanotechnol.* **12**, 907–913 (2017).
39. Z. Guo-Ping, L. Ying-Qiu, Y. Jie, C. Kai-Yu, Antibacterial characteristics of orange pigment extracted from Monascus pigments against Escherichia coli. *Czech J. Food Sci.* **34**, 197–203 (2016).
40. G. Grass, C. Rensing, M. Solioz, Metallic copper as an antimicrobial surface. *Appl. Environ. Microbiol.* **77**, 1541–1547 (2011).
41. A. Lange *et al.*, Silver and copper nanoparticles inhibit biofilm formation by mastitis pathogens. *Animals (Basel)* **11**, 1884 (2021).
42. I. M. Famuyide, F. O. Fasina, J. N. Eloff, L. J. McGaw, The ultrastructural damage caused by Eugenia zeyheri and Syzygium legatii acetone leaf extracts on pathogenic Escherichia coli. *BMC Vet. Res.* **16**, 326 (2020).
43. M. M. Mohamed, S. A. Fouad, H. A. Elshoky, G. M. Mohammed, T. A. Salaheldin, Antibacterial effect of gold nanoparticles against *Corynebacterium pseudotuberculosis*. *Int. J. Vet. Sci. Med.* **5**, 23–29 (2017).
44. K. S. Suganya *et al.*, Blue green alga mediated synthesis of gold nanoparticles and its antibacterial efficacy against Gram positive organisms. *Mater. Sci. Eng. C* **47**, 351–356 (2015).

45. L. Yang, W. Yan, H. Wang, H. Zhuang, J. Zhang, Shell thickness-dependent antibacterial activity and biocompatibility of gold@ silver core–shell nanoparticles. *RSC Advances* **7**, 11355–11361 (2017).
46. G. A. Sotiriou *et al.*, Nanosilver on nanostructured silica: Antibacterial activity and Ag surface area. *Chem. Eng. J.* **170**, 547–554 (2011).
47. M. Vincent, R. E. Duval, P. Hartemann, M. Engels-Deutsch, Contact killing and antimicrobial properties of copper. *J. Appl. Microbiol.* **124**, 1032–1046 (2018).
48. V. Govind *et al.*, Antiviral properties of copper and its alloys to inactivate covid-19 virus: a review. *Biometals* **34**, 1217–1235 (2021).
49. N. van Doremalen *et al.*, Aerosol and surface stability of SARS-CoV-2 as compared with SARS-CoV-1. *N. Engl. J. Med.* **382**, 1564–1567 (2020).
50. S. Cheeseman *et al.*, Antimicrobial metal nanomaterials: From passive to stimuli-activated applications. *Adv. Sci. (Weinh.)* **7**, 1902913 (2020).
51. S. M. Dizaj, F. Lotfipour, M. Barzegar-Jalali, M. H. Zarrintan, K. Adibkia, Antimicrobial activity of the metals and metal oxide nanoparticles. *Mater. Sci. Eng. C* **44**, 278–284 (2014).
52. R. H. Stauber *et al.*, Small meets smaller: Effects of nanomaterials on microbial biology, pathology, and ecology. *ACS Nano* **12**, 6351–6359 (2018).
53. N. Hutasoit *et al.*, Sars-CoV-2 (COVID-19) inactivation capability of copper-coated touch surface fabricated by cold-spray technology. *Manuf. Lett.* **25**, 93–97 (2020).
54. S. Raha, R. Mallick, S. Basak, A. K. Duttaroy, Is copper beneficial for COVID-19 patients? *Med. Hypotheses* **142**, 109814 (2020).
55. P. Bleichert, C. Espírito Santo, M. Hanczaruk, H. Meyer, G. Grass, Inactivation of bacterial and viral biothreat agents on metallic copper surfaces. *Biometals* **27**, 1179–1189 (2014).
56. S. Kumar *et al.*, Photoactive antiviral face mask with self-sterilization and reusability. *Nano Lett.* **21**, 337–343 (2021).
57. A. Kumar *et al.*, Copper@ ZIF-8 core-shell nanowires for reusable antimicrobial face masks. *Adv. Funct. Mater.* **31**, 2008054 (2020).
58. D. Maltoni, D. Maio, A. K. Jain, S. Prabhakar, *Handbook of Fingerprint Recognition* (Springer Science & Business Media, 2009).
59. W. DeFlorio *et al.*, Recent developments in antimicrobial and antifouling coatings to reduce or prevent contamination and cross-contamination of food contact surfaces by bacteria. *Compr. Rev. Food Sci. Food Saf.* **20**, 3093–3134 (2021).
60. E. A. Grice, J. A. Segre, The skin microbiome. *Nat. Rev. Microbiol.* **9**, 244–253 (2011).
61. D. Filingeri, Neurophysiology of skin thermal sensations. *Compr. Physiol.* **6**, 1429 (2016).
62. Q. Li *et al.*, Highly thermal-wet comfortable and conformal silk-based electrodes for on-skin sensors with sweat tolerance. *ACS Nano* **15**, 9955–9966 (2021).
63. S. Lee *et al.*, Nanomesh pressure sensor for monitoring finger manipulation without sensory interference. *Science* **370**, 966–970 (2020).
64. V. S. Hertzberg, Y. A. Wang, L. K. Elon, D. W. Lowery-North, The risk of cross infection in the emergency department: A simulation study. *Infect. Control Hosp. Epidemiol.* **39**, 688–693 (2018).
65. D. Pang, Y. Xiao, X.-Q. Zhao, A cross-infection model with diffusive environmental bacteria. *J. Math. Anal. Appl.* **9**, 125637 (2021).
66. T. J. Cho *et al.*, Underestimated risks of infantile infectious disease from the caregiver's typical handling practices of infant formula. *Sci. Rep.* **9**, 9799 (2019).
67. S. Cai, P. Ke, T. Narumi, K. Zhu, "Thermairglove: A pneumatic glove for thermal perception and material identification in virtual reality" in *2020 IEEE Conference on Virtual Reality and 3D User Interfaces (VR)* (IEEE, 2020), pp. 248–257.
68. I. Colombo *et al.*, HaCaT cells as a reliable in vitro differentiation model to dissect the inflammatory/repair response of human keratinocytes. *Mediators Inflamm.* **2017**, 7435621 (2017).
69. J. López-García, M. Lehocký, P. Humpolíček, P. Sáha, HaCaT keratinocytes response on antimicrobial atelocollagen substrates: Extent of cytotoxicity, cell viability and proliferation. *J. Funct. Biomater.* **5**, 43–57 (2014).
70. P. Slemming-Adamsen, J. Song, M. Dong, F. Besenbacher, M. Chen, In situ cross-linked PNIPAM/gelatin nanofibers for thermo-responsive drug release. *Macromol. Mater. Eng.* **300**, 1226–1231 (2015).